Simulating High-Latitude E-Region Irregularities using a 3D Fluid Framework with Kinetic Corrections

Yizhe Zhang, Roger H. Varney | UCLA Atmospheric and Oceanic Sciences

1. E-region Type-I Irregularities

- Type-I irregularities arise from the Farley-Buneman two-stream instability.
- Occur in strong-field electrojets near 110 km.
- Localized parallel electric fields drive anomalous electron heating.
- Affect high-latitude current closure pattern.

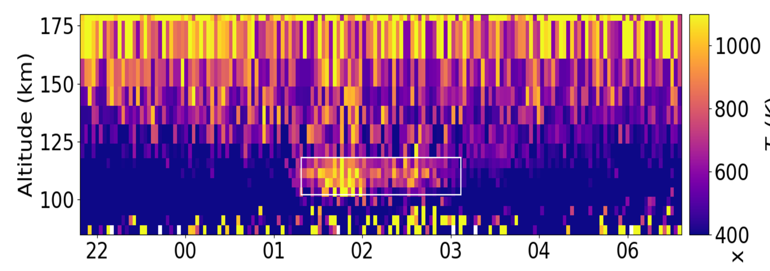

Fig 1: typical anomalous electron heating RTI observed by Poker Flat Incoherent Scatter Radar

Approximate two-stream threshold

$$|\mathbf{u}_e - \mathbf{u}_i| > C_s$$

2. Model framework and simulation configuration

A 3D five-moment fluid model with Fourier electron heat flux, Poisson closure, and realistic electron-mass ordering.

$$\underbrace{\frac{\partial n_i}{\partial t} + \nabla\cdot(n_i\mathbf{u}_i) = 0}_{\text{ion continuity}} \qquad \underbrace{\frac{\partial n_e}{\partial t} + \nabla\cdot(n_e\mathbf{u}_e) = 0}_{\text{electron continuity}} \qquad \underbrace{\nabla^2\Phi}_{\text{Poisson closure}} = \underbrace{-\frac{e(n_i - n_e)}{\epsilon_0}}_{\text{charge density}}$$

$$\underbrace{\frac{\partial \mathbf{u}_i}{\partial t} + (\mathbf{u}_i\cdot\nabla)\mathbf{u}_i}_{\text{ion inertia}} = \underbrace{-\frac{k_B}{m_i n_i}\nabla(n_i T_i)}_{\text{pressure force}} + \underbrace{\frac{q_i}{m_i}(\mathbf{E}_0 - \nabla\Phi + \mathbf{u}_i\times\mathbf{B}_0)}_{\text{electric + magnetic force}} - \underbrace{\nu_{in}\mathbf{u}_i}_{\text{neutral drag}} + \underbrace{\frac{1}{m_i n_i}\nabla\cdot\left[\frac{n_i k_B T_i}{\nu_{in}}\left(\nabla\mathbf{u}_i + (\nabla\mathbf{u}_i)^T - \frac{2}{3}(\nabla\cdot\mathbf{u}_i)\mathbf{I}\right)\right]}_{\text{emulated ion Landau damping}}$$

$$0 = \underbrace{-\frac{k_B}{n_e}\nabla(n_e T_e)}_{\text{pressure force}} \underbrace{-e(\mathbf{E}_0 - \nabla\Phi)}_{\text{electric force}} \underbrace{-e(\mathbf{u}_e\times\mathbf{B}_0)}_{\text{magnetic force}} \underbrace{-m_e\nu_{en}\mathbf{u}_e}_{\text{neutral drag}}$$

$$\underbrace{\frac{\partial T_i}{\partial t}}_{\text{temperature evolution}} + \underbrace{\mathbf{u}_i\cdot\nabla T_i}_{\text{thermal advection}} + \underbrace{\frac{2}{3}T_i\nabla\cdot\mathbf{u}_i}_{\text{compression heating/cooling}} = \underbrace{\frac{2\mu_{in}\nu_{in}}{3k_B}|\mathbf{u}_i|^2}_{\text{frictional heating}} - \underbrace{\delta_{in}\nu_{in}(T_i - T_n)}_{\text{neutral cooling}}$$

$$\underbrace{\frac{\partial T_e}{\partial t}}_{\text{temperature evolution}} + \underbrace{\mathbf{u}_e\cdot\nabla T_e}_{\text{thermal advection}} + \underbrace{\frac{2}{3}T_e\nabla\cdot\mathbf{u}_e}_{\text{compression heating/cooling}} = \underbrace{\chi_{e\perp}\nabla_\perp^2 T_e + \chi_{e\parallel}\frac{\partial^2 T_e}{\partial z^2}}_{\text{anisotropic heat conduction}} + \underbrace{\frac{2m_e\nu_{en}}{3k_B}|\mathbf{u}_e|^2}_{\text{Joule heating}} - \underbrace{\frac{T_e - T_{K,\parallel}}{\tau_E}}_{\text{parallel kinetic heating feedback}}$$

- Poisson closure allows charge accumulation.
- Realistic electron mass, which directly affects linearly unstable aspect angle range, is retained in mobility and heating coefficients.
- Neglecting electron inertia term, has little effect on nonlinear saturation, and saves runtime.

Kinetic closure

Reduced kinetic closures are added where five-moment fluid theory is no longer valid.

Parallel heating

$$-\frac{T_e - T_{K,\parallel}(E_{\parallel,\mathrm{rms}})}{\tau_E}$$

Non-Maxwellian heating feedback.

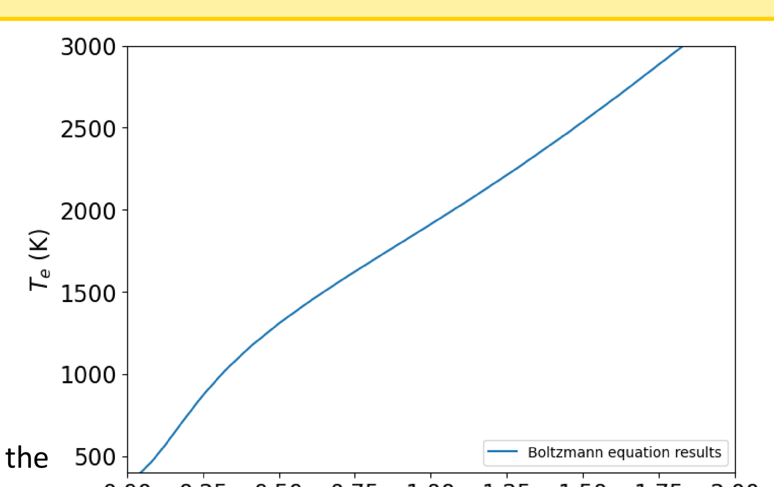

Fig 2. Electron heating increases strongly with the turbulent parallel electric field.

Ion Landau damping

$$\mathbf{V}_i = \frac{1}{m_i n_i}\nabla\cdot\left[\frac{n_i k_B T_i}{\nu_{in}}\mathbf{S}_i\right]$$

$$\mathbf{S}_i = \nabla\mathbf{u}_i + (\nabla\mathbf{u}_i)^T - \frac{2}{3}(\nabla\cdot\mathbf{u}_i)\mathbf{I}$$

High-k damping from ion viscosity.

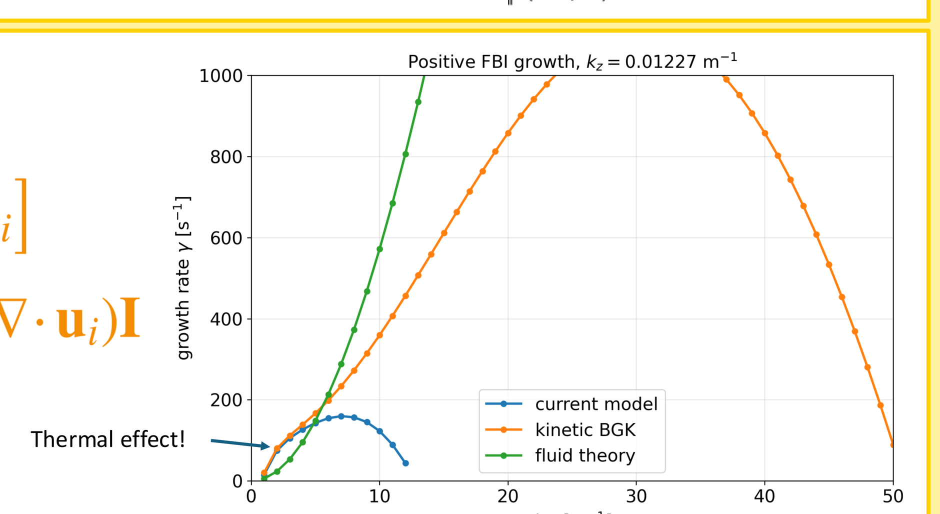

Fig 3. Linear growth comparison between the current model, kinetic BGK theory, and fluid theory.

Numerical methods

Dedalus v2 Fourier pseudospectral solver with periodic boundaries.

- 3D Fourier domain
- 3/2 nonlinear dealiasing
- IMEX RK222
- linear terms implicit, nonlinear fluxes explicit
- adaptive timestep from ion and delta E x B CFL limits

Simulation configuration

Domain	12 x 12 x 2048 m
Grid	180 x 180 x 48
E0	60 mV/m
B0	5e-5 T
n0	1e11 m^-3
Tn, Ti0, Te0	348 K
nu_in, nu_en	1e3, 2e4 s^-1
mi, me	30 mp, realistic

Takeaway: kinetic-informed heating and high-k damping are embedded in a fast 3D fluid solver.

3. Results: 3D evolution, heating, and observational signatures

Three-stage turbulent evolution

- Linear growth → intermediate cascade → nonlinear saturation

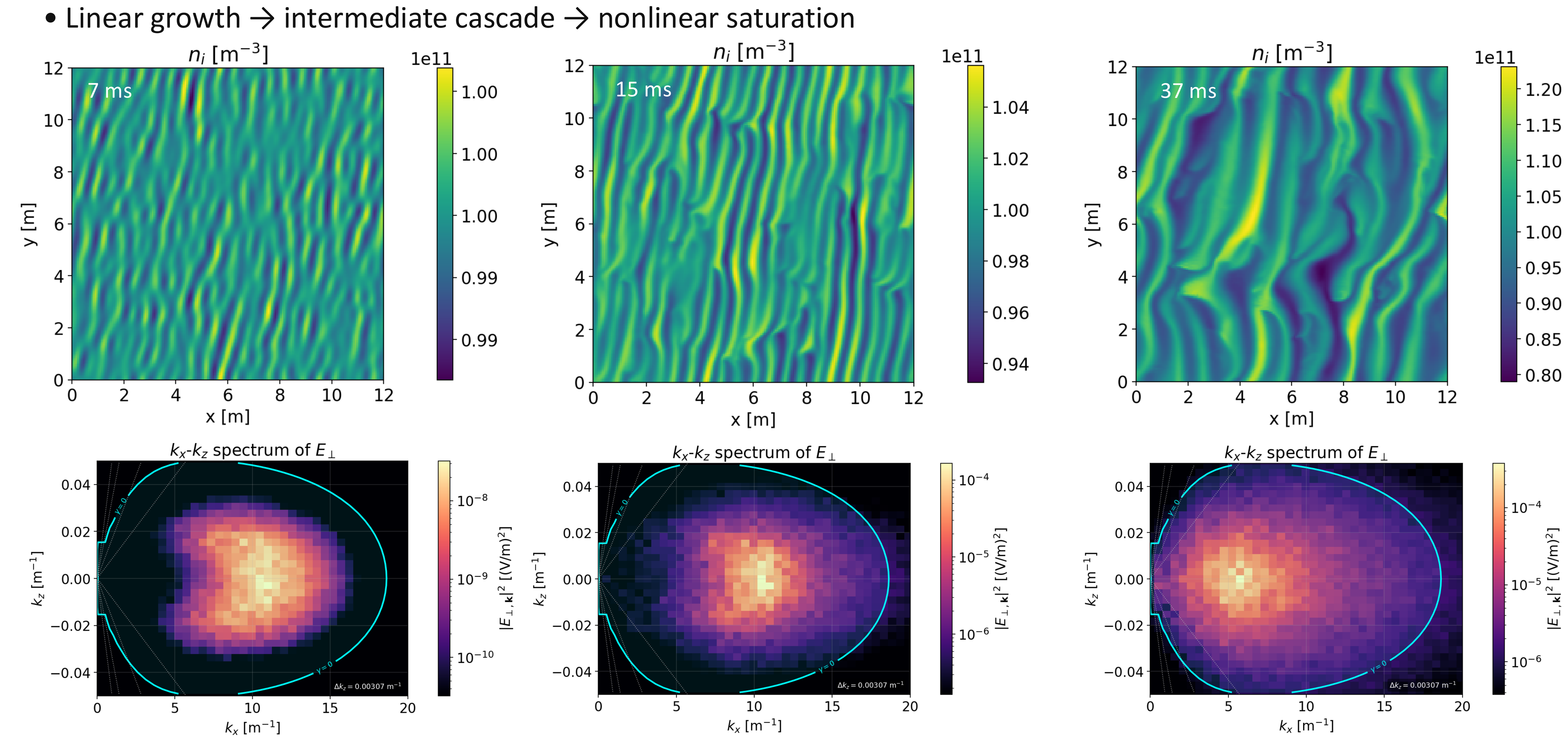

Fig 4. Density structures and electric fieldspectral evolution from linear growth to nonlinear turbulence. The x direction is the cross-field drift direction, and the y direction is the driving electric-field direction.

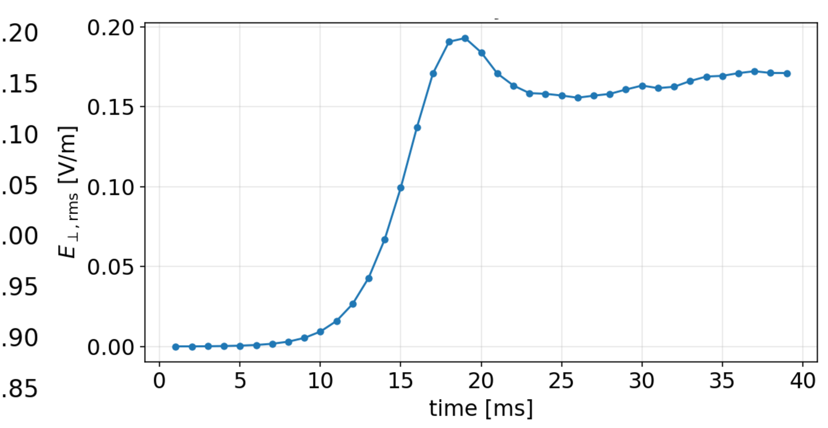

Fig 5. History of RMS turbulent perpendicular electric field. Grows rapidly, then approaches a saturated level.

Spectral evolution and aspect-angle cascade

- Inverse cascade, dominant wavelength is longer than the fastest growing mode; Final spectrum consistent with weak coupling prediction.
- Aspect-angle cascade channels wave energy into parallel electric fields, producing a 3D heating pathway.
- Te RMS: steep rise from aspect-angle cascade; slower rise from further inverse cascade.

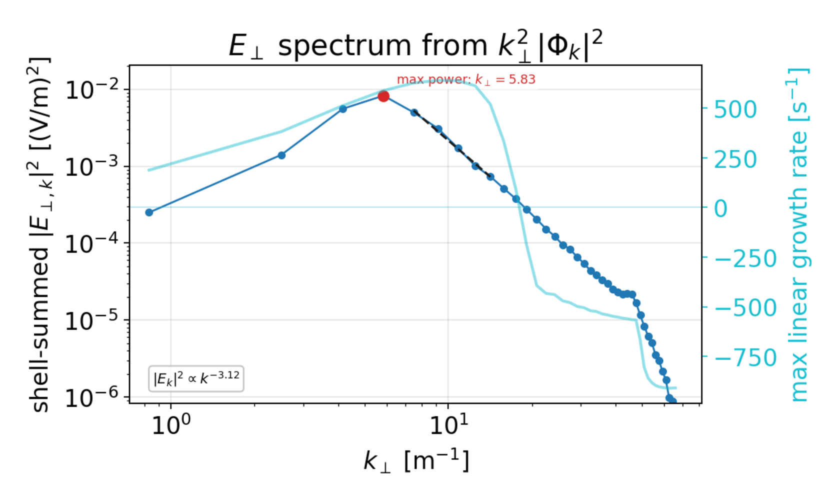

Fig 6. Saturated perpendicular electric-field spectrum.

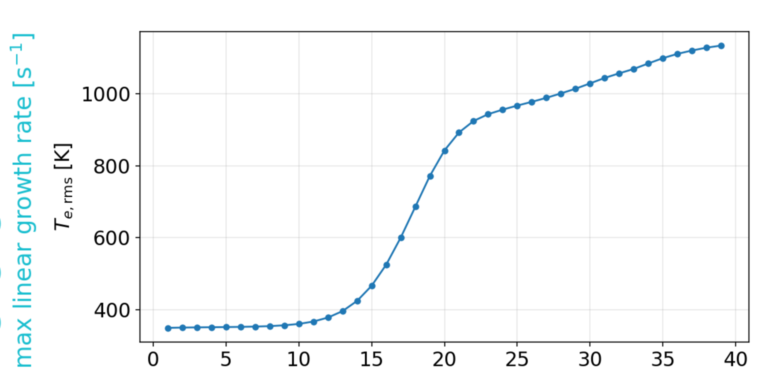

Fig 7. RMS electron temperature time history.

Current limitations

- Missing nonlinear kinetic effects such as nonlinear Landau damping
- Finite box size may affect inverse cascade and large-scale energy storage
- Emulated Landau damping slightly modifies linear growth

Comparisons to observations

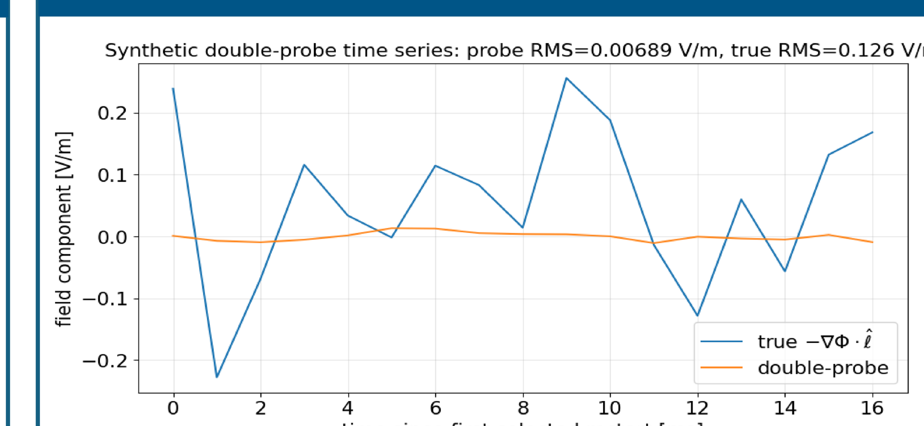

Fig 8. Synthetic double-probe sampling shows that rocket-like measurements can underestimate the true turbulent electric field.

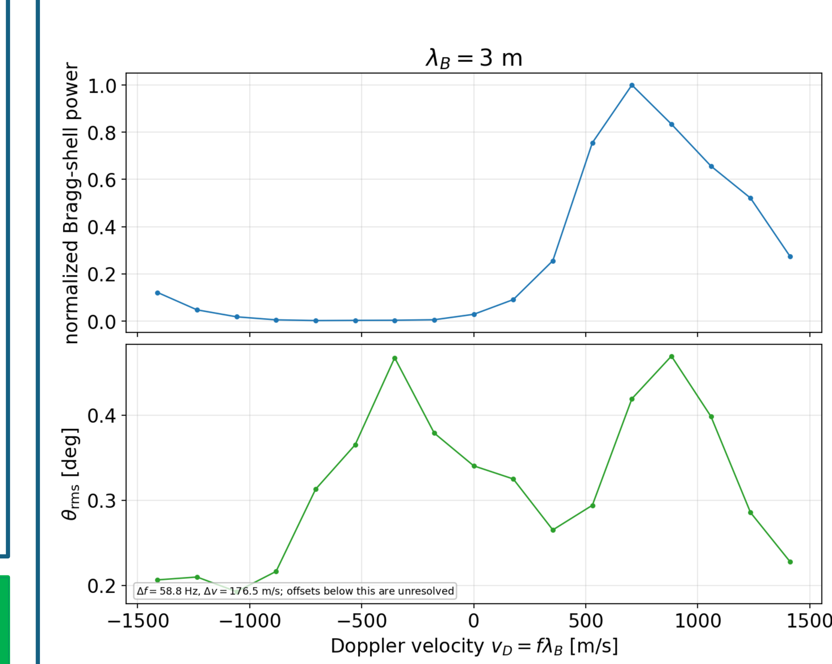

Fig 9. Synthetic VHF radar diagnostic showing Bragg-scale power and RMS aspect angle.

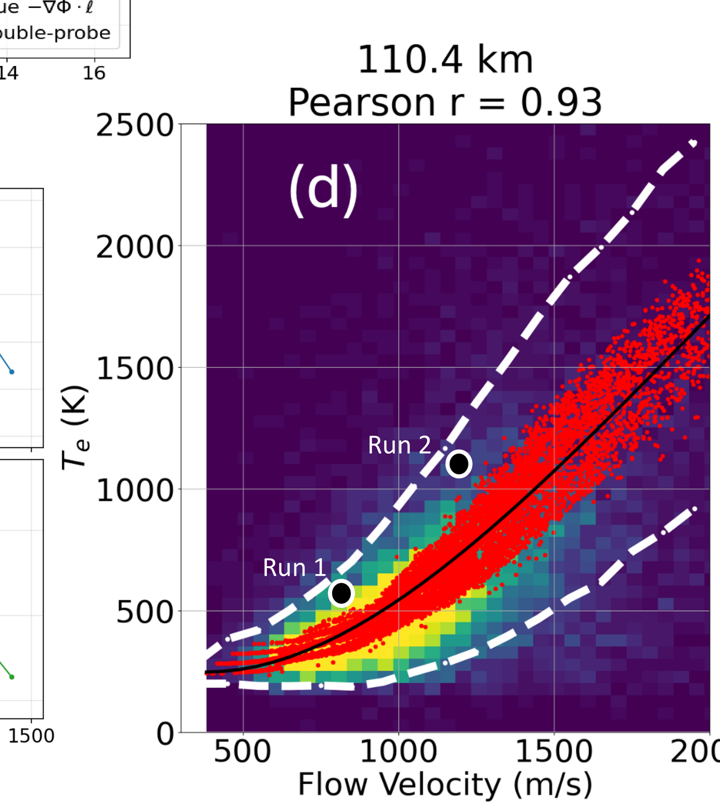

Fig 10. Simulation cases compared with observed electron heating versus flow speed at 110.4 km.

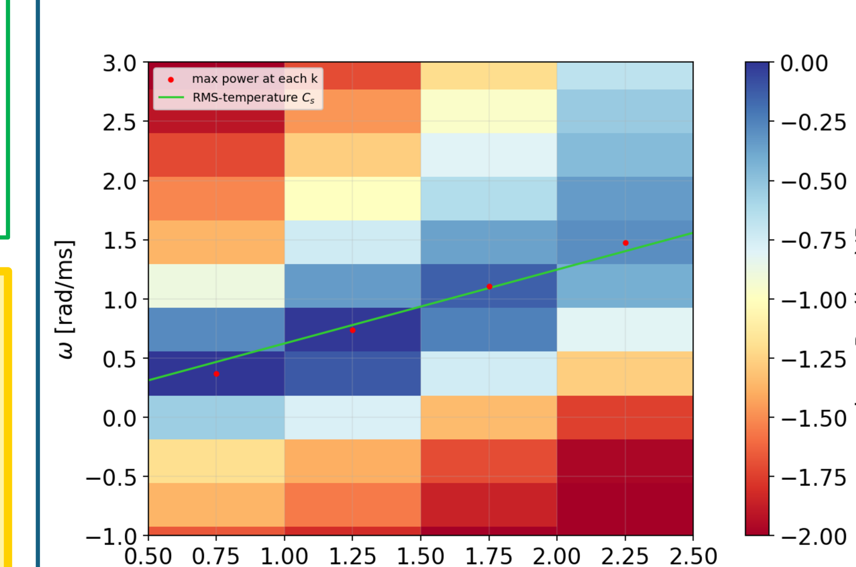

Fig 11. Synthetic radar spectrum showing observation-like phase speeds in the simulated turbulence.

- Synthetic double-probe field gives observation-like RMS E (7 mV/m)
- RMS aspect angle: ~0.4° (consistent)
- Electron temperature reaches ~1100 K (consistent)
- Phase velocity is consistent with observations (ion acoustic speed).

Conclusions

- A new 3D fluid model framework with kinetic closures is proposed.
- Realistic electron mass is proven to be important in simulating FB turbulence.
- Aspect-angle cascade redirects wave energy toward finite parallel k, enhancing electron heating and making the system more dissipative, which helps saturation.
- Synthetic rocket diagnostics are essential: the “measured” field can differ strongly from the true simulation RMS.
- The model reaches observation-like electron temperatures, phase speeds, and aspect angles, but nonlinear kinetic saturation remains the main missing physics.

Acknowledgement: YZ is supported by the NSF grant AGS-2442522. RHV is supported by the NSF Faculty Development in Space Sciences award AGS-1936186.